Matteo Vecellio,[1,2] Francesco Spallotta,[1,2] Simona Nanni,[3] Claudia Colussi,[3] Chiara Cencioni,[2] Anja Derlet,[4] Beatrice Bassetti,[1] Manuela Tilenni,[1] Maria Cristina Carena,[1,2] Antonella Farsetti,[5] Gianluca Sbardella,[6] Sabrina Castellano,[6] Antonello Mai,[7] Fabio Martelli,[8] Giulio Pompilio,[1] Maurizio C. Capogrossi,[9] Alessandra Rossini,[10] Stefanie Dimmeler,[4] Andreas Zeiher,[11] and Carlo Gaetano[2]

# The Histone Acetylase Activator Pentadecylidenemalonate 1b Rescues Proliferation and Differentiation in the Human Cardiac Mesenchymal Cells of Type 2 Diabetic Patients

*Diabetes 2014;63:2132–2147 | DOI: 10.2337/db13-0731*

COMPLICATIONS

**This study investigates the diabetes-associated alterations present in cardiac mesenchymal cells (CMSC) obtained from normoglycemic (ND-CMSC) and type 2 diabetic patients (D-CMSC), identifying the histone acetylase (HAT) activator pentadecylidenemalonate 1b (SPV106) as a potential pharmacological intervention to restore cellular function. D-CMSC were characterized by a reduced proliferation rate, diminished phosphorylation at histone H3 serine 10 (H3S10P), decreased differentiation potential, and premature cellular senescence. A global histone code profiling of D-CMSC revealed that acetylation on histone H3 lysine 9 (H3K9Ac) and lysine 14 (H3K14Ac) was decreased, whereas the trimethylation of H3K9Ac and lysine 27 significantly increased. These observations were paralleled by a downregulation of the GCN5-related N-acetyltransferases (GNAT) p300/CBP-associated factor and its isoform 5-α general control of amino acid synthesis (GCN5a), determining a relative decrease in total HAT activity. DNA CpG island hypermethylation was detected at promoters of genes involved in cell growth control and genomic stability. Remarkably, treatment with the GNAT proactivator SPV106 restored normal levels of H3K9Ac and H3K14Ac, reduced DNA CpG hypermethylation, and recovered D-CMSC proliferation and differentiation. These results suggest that epigenetic interventions may reverse alterations in human CMSC obtained from diabetic patients.**

In recent decades, in association with the progressive increase of the average population age in western countries, type 2

[1]Laboratorio di Biologia Vascolare e Medicina Rigenerativa, Centro Cardiologico Monzino, Milan, Italy
[2]Division of Cardiovascular Epigenetics, Department of Cardiology, Goethe University, Frankfurt am Main, Germany
[3]Institute of Medical Pathology, Catholic University of Rome, Policlinico A. Gemelli, Rome, Italy
[4]Institute of Cardiovascular Regeneration, Goethe University, Frankfurt am Main, Germany
[5]Consiglio Nazionale delle Ricerche, Institute of Cellular Biology and Neurobiology, Rome, Italy
[6]Department of Pharmaceutical and Biomedical Sciences, University of Salerno, Fisciano (SA), Italy
[7]Department of Drug Chemistry and Technology, University of Rome, Rome, Italy
[8]Istituto di Ricovero e Cura a Carattere Scientifico Policlinico San Donato, Laboratorio di Cardiologia Molecolare, San Donato Milanese, Milan, Italy
[9]Laboratorio di Patologia Vascolare, Istituto Dermopatico dell'Immacolata, Rome, Italy
[10]Department of Clinical Sciences and Community Health, University of Milano, Milan, Italy
[11]Internal Medicine Clinic III, Department of Cardiology, Goethe University, Frankfurt am Main, Germany

Corresponding author: Carlo Gaetano, carlo.gaetano@gmail.com or gaetano@em.uni-frankfurt.de.

Received 7 May 2013 and accepted 14 January 2014.

This article contains Supplementary Data online at http://diabetes.diabetesjournals.org/lookup/suppl/doi:10.2337/db13-0731/-/DC1.

M.V., F.S., and S.N. contributed equally to this work.

M.V. and M.C.Car. are currently affiliated with the University of Oxford, Institute of Musculoskeletal Sciences, Botnar Research Centre, Nuffield Department of Orthopaedics, Rheumatology and Musculoskeletal Sciences, Nuffield Orthopaedic Centre, Oxford U.K.



**See accompanying article, p. 1841.**

diabetes (T2D) and its complications have gained worldwide relevance. It is now evident, in fact, that age, lifestyle, and behavioral factors play a pivotal role in the determination of T2D risk, reinforcing the indication of T2D as a metabolic disorder conditioned by genetic and environmental factors (1).

The most common complications of diabetes include acidosis, micro- and macrovascular angiopathy, atherosclerosis, neuropathy, retinopathy, and kidney disease (2). Cardiovascular accidents, however, represent a growing cause of death for diabetic patients. Several recent studies, in fact, indicate that the mortality risk in diabetic patients who have an acute myocardial infarction is about double that of normoglycemic patients (3).

β-Blockers, thrombolytic agents, aspirin, ACE inhibitors, and lipid-lowering drugs are the most commonly used therapeutics for the treatment of diabetic patients who sustain an acute myocardial infarction. During the acute cardiac event, metabolic control is also considered of major importance because of the increase in fatty acid metabolism that may compromise glycolysis in ischemic and nonischemic areas, further worsening cardiac function (4).

Accordingly, a growing body of evidence suggests that T2D alters cellular functions, including those of adult stem cells (5,6). For instance, circulating endothelial progenitor cells, essential in vasculogenesis, wound healing, and for the revascularization of the ischemic heart, are compromised in their regeneration potential (7). As well, cardiomyocytes and cardiac vascular cells appear all functionally impaired after the onset of diabetes (8).

We recently characterized a human cardiac-specific mesenchymal cell (CMSC) population isolated from the cardiac auricles (9) of donor patients undergoing surgery for coronary artery bypass grafting (CABG) (9). These cells revealed the presence of typical mesenchymal surface markers (10), the ability to differentiate along the osteogenic, adipogenic, and vasculogenic lineages, and when injected in a rat infarcted heart, they contributed to the formation of vessels and new cardiomyocytes (9). Under chemically controlled conditions, these cells could be epigenetically reprogrammed to obtain functionally competent cardiovascular precursors with electrophysiology, gene expression, and microRNA profile similar to that of cardiomyocyte progenitors (11). Noteworthy, during the progress of these studies, we found that CMSC obtained from diabetic patients (D-CMSC) had a lower proliferation rate and failed to reprogram, suggesting the presence of a functional impairment (11,12).

In this report, we describe epigenetic alterations, predominantly characterized by histone hypoacetylation and DNA hypermethylation at promoter CpG islands, detectable in T2D-derived human CMSC. These defects were associated with a reduced proliferation and differentiation potential. Remarkably, the histone acetylase (HAT) activator pentadecylidenemalonate 1b (SPV106) (12), known to accelerate wound healing (13), rescued the epigenetic defects and restored a nearly normal chromatin structure and CpG methylation of cell cycle and DNA repair genes with a significant rescue in proliferation and differentiation. These results provide the first evidence that a targeted epigenetic intervention may restore function in adult cardiac stromal cells from T2D patients.

## RESEARCH DESIGN AND METHODS

### Patients

The current study enrolled 22 patients (see Supplementary Table 1) undergoing CABG or angioplasty. Clinical information collected for each patient included age, sex, diabetes onset, postischemia heart revascularization, and medical treatments before surgery (see Supplementary Table 2). All patients were enrolled after ethical committee approval and signed informed consent. Investigations were conducted according to the principles expressed in the Declaration of Helsinki. Data were analyzed anonymously.

### CMSC Isolation and Culture

CMSC from normoglycemic donors (ND-CMSC) and diabetic donors (D-CMSC) were isolated from the right auricles of the patients and cultured in growth medium, as previously described (9).

### Western Blot Analysis

ND-CMSC and D-CMSC cell extracts were prepared as described previously (9). Briefly, proteins were resolved by SDS-PAGE, transferred onto nitrocellulose membrane (Bio-Rad), and incubated overnight at 4°C with the antibodies listed in Supplementary Table 3. Each filter was reprobed with anti–β-actin or antihistone H3/antihistone H4 to verify equal protein loading. Densitometry was performed by National Institutes of Health image software.

### Quantitative Real-Time PCR

RNA isolation was performed with TRIzol (Invitrogen). cDNA synthesis was prepared with a High-Capacity cDNA Archive kit (Applied Biosystems). Quantitative PCR (qPCR) was performed with the ABI Prism 7500 and 7900HT Fast Real-Time PCR instruments (Applied Biosystems) using SYBR Master Mix (Applied Biosystems) with evaluation of dissociation curves. mRNA levels of each gene were quantified using the standard curve method (5 log dilutions in triplicate) and expressed relative to housekeeping 18S rRNA and/or β-actin genes. Predesigned TaqMan primers and probe (Applied Biosystems) specific for β-actin and 18S rRNA, and the following custom-designed primers were used:

hBRCA1 forward (F) 5′-CCACTCAGCAGAGGGATACCA-3′;
hBRCA1 reverse (R) 5′-TTATGATGGAAGGGTAGCTGTTA GAA-3′;
hBRCA2 F 5′-TCAGCTTACTCCGGCCAAAA-3′;
hBRCA2 R 5′-ACGATATTCCTCCAATGCTTGGT-3′;
hTP53 F 5′-GCCTGAGGTTGGCTCTGACT-3′;
hTP53 R 5′-CCATGCAGGAACTGTTACACATG-3′;
hCCNF F 5′-GCGTCTTGAGCCTCCATAAGAA-3′;

hCCNF R 5′-CACGGCGGTCAGAGAGACTT-3′;
hCCNA1 F 5′-GTACTTGAGGCGACAAGGAGTGT-3′;
hCCNA1 R 5′-GTAGACTCAGCTCTGCTACGTACTTAGC-3′;
hCCNB1 F 5′-TGTCTCCATTATTGATCGGTTCA-3′;
hCCNB1 R 5′-CCAACCAGCTGCAGCATCT-3′;
PCAF F 5′-CCGTGAAGAAAGCGCAACTAC-3′;
PCAF R 5′-AGACTCCTCGGCCTTGCA-3′.

### PCR Array Profile

Total RNA was extracted using the RNeasy Mini kit (Qiagen, Toronto, Ontario, Canada). cDNA was synthesized from 1 μg of RNA with SuperScript III first strand synthesis (Life Technologies) in a 20-μL reaction volume. Primers were spotted in a plate from SABiosciences for epigenetic enzymes modifying chromatin, and real-time PCR was performed on Applied Biosystem ABI 7900 using SYBR Green ROX qPCR Mix (Qiagen). Quantification of gene expression was assessed with the comparative cycle threshold (Ct) method.

### Chromatin Immunoprecipitation

Chromatin immunoprecipitation was performed with ChIP-IT Express Enzymatic kit (Active Motif) according the manufacture's instruction using specific antibodies to histone H3 lysine 9 (H3K9Ac) and H3 lysine 9 monomethylation (H3K27me3; Abcam). Negative control was absence of antibody (noAb). DNA fragments were recovered and analyzed using quantitative method based on real-time PCR as described (14) by using the following primers:

hCCNA1 F 5′-GACAGGTTCCACGAACAAACAC-3′;
hCCNA1 R 5′-GAAACCTCACGCCCTTTTCC-3′;
hCCNB1 F 5′-GGCAGAGGAGAGCAAGGGTAA-3′;
hCCNB1 R 5′-TGGATCGTTATTGAGTCTTCTGTCA-3′;
hCCNF F 5′-CTTCTCTGAATGTGGGATTTCTCA-3′;
hCCNF R 5′-GGTGTCGGTTGAAAACGTTATG-3′;
hBRCA1 F 5′-CGTTGTCACCTCGCATTCTG-3′;
hBRCA1 R 5′-GGACCGAGTGGGCGAAA-3′;
hBRCA2 F 5′-CCCATGGGAGCAACTCTCA-3′;
hBRCA2 R 5′-CCGAATTCGTTGGTTCTGTAACA-3′;
hTP53 F 5′-TGAAAGCACTGTGTTCCTTAGCA-3′;
hTP53 R 5′-TCGGAAGGTGGACCGAAAT-3′.

### DNA Methylation Profiler and Methyl-DNA Immunoprecipitation Assay

Genomic DNA was extracted with DNeasy Blood and Tissue Kit (Qiagen) and 1,000 ng of DNA was used in the Methyl-Profiler DNA Methylation PCR Array System, specific for Cell Cycle (no. cat 335211 SABiosciences). Genomic DNA was digested with methylation-sensitive and methylation-dependent enzymes, as described in the protocol. The assay was performed following manufacturer's instructions supplied by the kit. Real-time PCR was executed with specific cycling conditions as indicated in the manual. Data analysis was conducted following the instructions of the SABiosciences Web site (http://www.sabiosciences.com/methylationdataanalysis.php). DNA for the methyl-DNA immunoprecipitation (MeDIp) assay was prepared from cross-linked chromatin, as previously described (15). Purified DNA (500–800 ng) was denatured and methylation analysis performed with MeDIP kit (Active Motif), according the manufacturer's instructions, using a specific monoclonal antibody to 5-methylcytosine or mouse IgG as the negative control. Methylated DNA was analyzed by PCR using the primers listed above.

### HAT Activity

For each sample, 80 μg was used for the determination of HAT activity. The assay was performed following the manufacturer's instructions (BioVision).

### Acidic β-Galactosidase Assay

Senescence-associated acidic β-galactosidase was assayed following the manufacturer's instructions (Cell Signaling Technology).

### Matrigel Tube Formation Assay

Matrigel (200 μL) was placed on 24-well plates and incubated at 37°C for 1 h. Then, $5 \times 10^4$ cells were plated on Cultrex and incubated for 1 to 7 h. Capillary-like structure density was examined by phase-contrast microscopy.

### Immunofluorescence

Cells were fixed with 4% paraformaldehyde for 10 min. Blocking buffer (BSA at 5% in PBS solution) was added for 1 h at room temperature. Primary antibodies H3K9Ac and H3K27me3 were incubated overnight at 4°C in a moisture chamber. Nuclei were counterstained by DAPI. Images were collected with an Axio Observer Z1 microscope equipped with the ApoTome deconvolution system and AxioVision software (Zeiss). Samples for confocal analysis were analyzed by using a Zeiss LSM 510 Meta Confocal Microscope with original magnification ×40 or ×80. Laser power, beam splitters, filter settings, pinhole diameters, and scan mode were the same for all examined fields of each sample. Negative immunofluorescence control was performed using normal rabbit or mouse IgG instead of the specific rabbit or mouse primary antibody.

### Extracellular Flux Analysis

Kinetic metabolic profiling was done in real time by the fully integrated 96-well Seahorse Bioscience XF$^e$96 Extracellular Flux Analyzer (North Billerica, MA) by using the XF Cell Mito Stress Test Kit (Seahorse Bioscience, part # 102308-400) for determination of the oxygen consumption rate as a surrogate for mitochondrial respiration and the XF Glycolysis Stress Test Kit (Seahorse Bioscience, part # 102194-100) to determine the extracellular acidification rate for determining glycolytic capacity of the cells. CMCS ($3 \times 10^5$) were seeded for 3 h at 37°C in a XF96 Polystyrene Cell Culture Microplates (Seahorse Bioscience, part # 101085-004) in growth medium (20%

Iscove's modified Dulbecco's medium). After 3 h, the cells were washed with basal Dulbecco's modified Eagle's medium and cultured for 1 h at 37°C without $CO_2$ in mito and glycolysis stress assay media, as from the manufacturer described (Seahorse Bioscience). Afterward, metabolic profiles were determined by adding oligomycin (2 μmol/L), carbonylcyanide-4-(trifluoromethoxy)-phenylhydrazone (FCCP; 2 μmol/L), antimycin (2 μmol/L) and rotenone (1 μmol/L) for the oxygen consumption rate, and glucose (10 mmol/L), oligomycin (1 μmol/L), and 2-DG (1 mol/L) for the extracellular acidification rate. Data are presented as mean ± SEM of five ND-CMSC and four D-CMSC ($P \leq 0.05$), determined by the Student *t* test.

### Statistics

Statistical analysis was performed using ANOVA or the Student *t* test. $P \leq 0.05$ was considered significant.

## RESULTS

### Isolated ND-CMSC and D-CMSC Show Distinct Proliferation Rates

CMSC were isolated from the auricles of normoglycemic and T2D patients, as previously described (9), and cultured in mesenchymal medium (9). The presence of mesenchymal markers including CD29, CD105, and CD73 and the absence of CD45, CD34, CD14, CD19, and HLA-DR was verified by fluorescence-activated cell sorter analysis, and no significant differences were noted between cells obtained from diabetic and normoglycemic patients (data not shown). A total of 22 CMSC strains were obtained from 11 ND-CMSC and 11 T2D patients (D-CMSC, see Supplementary Table 1). During the progress of this work and in consequence of their different growth rate, not all cell isolates could be analyzed in the experiments. All 22 strains were assayed for proliferation, and 8 ND-CMSC and 8 D-CMSC were analyzed for DNA methylation (see below). A variable number, ranging from two to six independent randomly chosen cellular strains from each patient group, was used in Western blot, senescence differentiation, gene expression, chromatin immunoprecipitation (ChIP) or MeDIp. Cells were cultured up to passage 8, and each experiment was repeated three times, with the exception of ChIP experiments, which were performed in double on two different cell groups in consequence of the limited sample availability.

D-CMSC evaluated at 3, 7, and 14 days of ex vivo culture showed reduction in growth of ~1.9-, 2.7-, and 3.5-fold compared with controls (Fig. 1*A*). In addition, D-CMSC had a flattened and elongated morphology and were positive for acidic β-galactosidase evaluated after 7 days of culture (Fig. 1*B*). To investigate whether the expression of cell cycle control elements was altered, protein level analysis was performed on different proliferation associated markers, including the proliferation cell nuclear antigen (PCNA) (16); the phosphorylation status of serine 10 on histone H3 (H3S10P), a posttranslation histone modification often associated with proliferating cells; the relative abundance of histone H3.3, a marker of active cell cycle S phase (17); and $p21^{wa61}$, a molecule involved in the negative regulation of cell cycle progression and in the onset of senescence (18). ND-CMSC and D-CMSC expressed a similar level of PCNA, but D-CMSC revealed a significant decrease in H3S10P (Fig. 1*A* and *C*). Moreover, the histone variant H3.3 was detectable only in ND-CMSC, further supporting the evidence that reduced proliferation occurred in D-CMSC (Fig. 1*C*). These modifications were paralleled by an increase in $p21^{wa61}$ and acidic β-galactosidase signals, underlying the onset of premature senescence in these cells (19).

### D-CMSC Are Impaired in Their Ex Vivo Differentiation Potential

Multilineage differentiation assays were performed to evaluate the potential of D-CMSC and ND-CMSC. In adipogenic medium (16), D-CMSC and ND-CMSC stained positive for Oil Red O; however, ND-CMSC developed a number of lipid drops higher than that of D-CMSC (Fig. 2*A*) and stored more lipids then D-CMSC, with average optical density D readings at 405 nm of 0.3 ± 0.05 for ND-CMSC and 0.22 ± 0.07 for D-CMSC ($P \leq 0.05$; Fig. 2*A*).

We previously reported that a designed epigenetic cocktail (EpiC) made of retinoid, phenylbutyrate, and a nitric oxide donor (11) induced a cardiac precursors-like phenotype in CMSC stimulating the expression of early cardiovascular markers. During the progress of the present work, a series of experiments were performed to explore D-CMSC versus ND-CMSC differentiation potential in response to EpiC (11). ND-CMSC upregulated cardiac stem cells markers, including c-Kit, KDR, and MDR-1 (17). D-CMSC, however, dramatically failed to do so (Fig. 2*B*).

Cultrex assay (Fig. 2*C*) was performed to evaluate CMSC vessel-like structure formation as an in vitro readout of their angiogenic potential. This property was significantly impaired in D-CMSC compared with ND-CMSC (average [SD] number of branches/field was 3.4 ± 0.7 for ND-CMSC and 0.9 ± 0.3 for D-CMSC).

### Chromatin Landscape Discriminates Between ND-CMSC and D-CMSC

Experiments aimed at exploring the chromatin landscape characterizing ND-CMSC and D-CMSC, were performed on the tails of histones H3 and H4. Several characterizing modifications were identified. Specifically in D-CMSC, an increase in H3K9Ac trimethylation (H3K9Me3) paralleled by a decrease in H3K9Me (Fig. 3*A*) and H3K9Ac and H3K14Ac was observed (Fig. 3*B*). These modifications are often associated with a closed chromatin structure less accessible to transcription factors and leading to gene repression. To further explore this possibility, we extended our evaluations to a larger number of histone modifications, including the Polycomb-dependent histone H3 repressive modification determined by the trimethylation of H3K27me3. H3K27me3 significantly increased in D-CMSC, as assessed by Western blot (Fig. 3*A*). Confocal

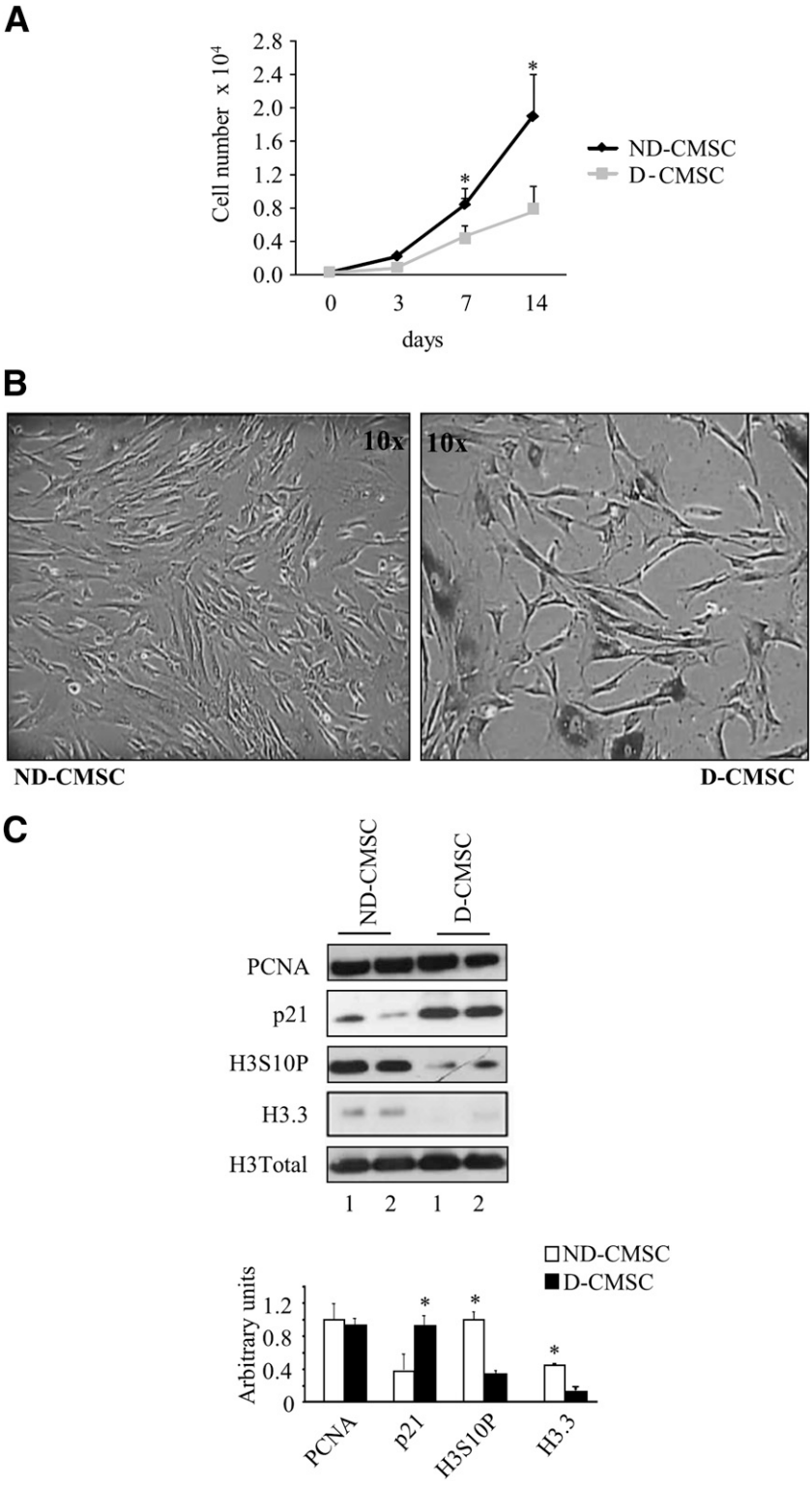


**Figure 1—**Proliferation analysis of ND-CMSC and D-CMSC. *A*: Growth curve of ND-CMSC and D-CMSC cultured in growth medium for 3, 7, and 14 days ($n$ = 11, for each group). *B*: Acidic β-galactosidase assay performed on ND-CMSC and D-CMSC after 7 days in culture ($n$ = 6 for each group). *C*: Western blot of proliferation markers PCNA, H3S10P, H3.3, and p21 in ND-CMSC and D-CMSC ($n$ = 4, for each group) grown in growth medium. The same filter was probed with total histone H3 to show equal nuclear protein loading. Band density is reported in the associated bar graph ($n$ = 4 for each group). *$P \leq 0.05$.

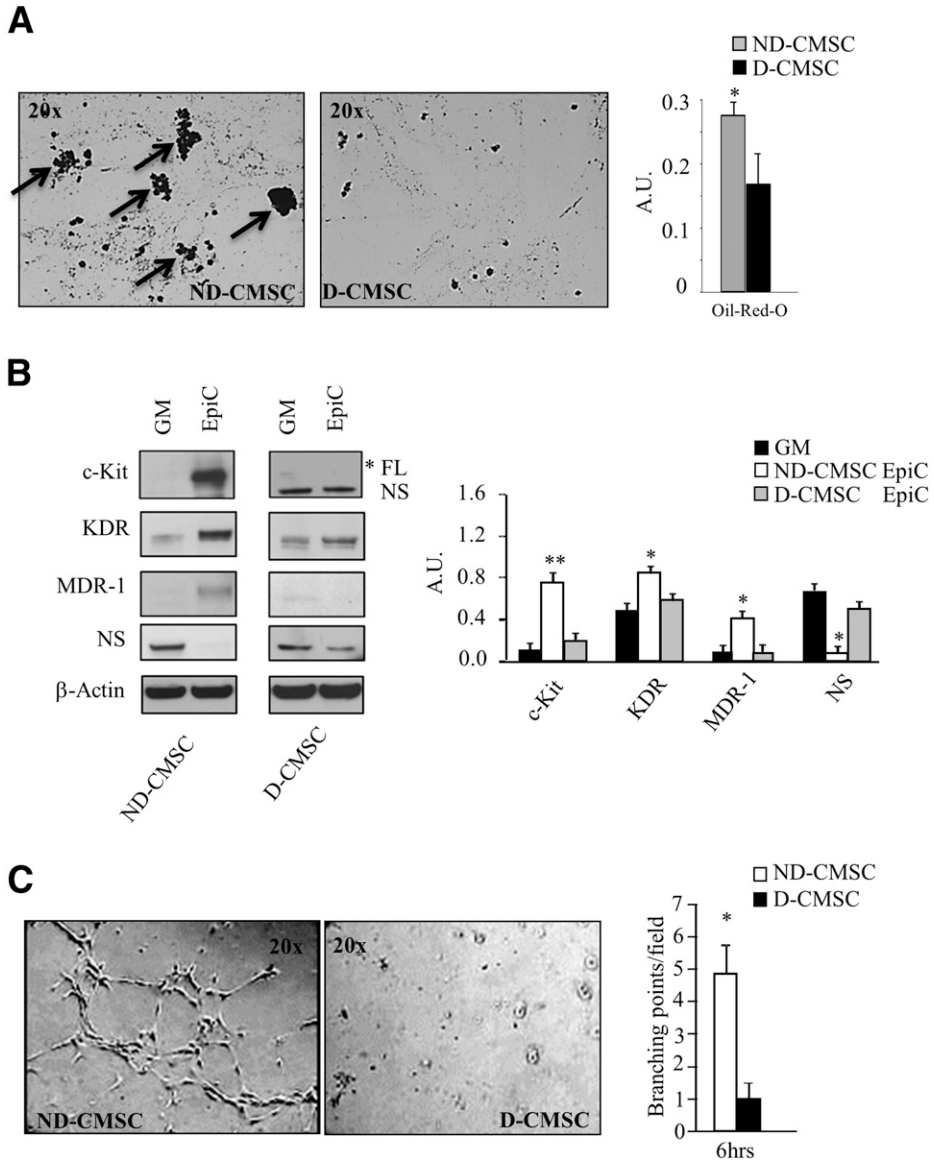


**Figure 2**—CMSC in vitro differentiation potential. *A*: The panel shows a representative picture of Oil Red O assay on ND-CMSC and D-CMSC after 21 days of treatment with the adipogenic medium, with the black arrows indicating lipid drops accumulation. The bar graph represents average lipid content evaluated in three independent experiments. Values in arbitrary units (A.U.) were obtained by spectrophotometer reading at 550 nm normalized to the number of cells. *B*: ND-CMSC and D-CMSC differentiation into cardiac precursors after EpiC treatment for 1 week. Western blot analysis shows expression of c-Kit, MDR-1, KDR, and nucleostemin (NS); the relative band density is represented in the bar graph ($n = 4$ for each group). GM, growth medium. *$P \leq 0.05$, **$P \leq 0.005$. *C*: The panel shows a representative picture of Cultrex assay on ND-CMSC (*left*) and D-CMSC (*right*) cultured in endothelial cell growth media-2 for 14 days. The bar graph shows quantification of capillary-like structure formation measured as the count of branching points per field ($n = 4$ for each group). *$P \leq 0.05$.

microscopy further confirmed the increase in H3K27me3 and the reduction in H3K9Ac in D-CMSC nuclei (Supplementary Fig. 1*A*). Similar results were obtained in the cardiomyocyte-derived HL-1 cell line (18) and in human umbilical vein–derived endothelial cells (HUVEC) exposed to high glucose (25 μmol/L) for 72 h (Supplementary Fig. 1*B* and Supplementary Fig. 3*A*).

Further histone code analyses showed a decrease in histone H4 lysine 16 acetylation (H4K16Ac) in D-CMSC, suggesting a generalized reduction in the activity of those enzymes deputed to lysine acetylation and chromatin opening (Fig. 3*D*). In these experiments, we found no significant differences in the monomethylation of histone H4 lysine 20 (H4K20Me), often associated with opened and accessible chromatin, whereas the trimethylation of H4 lysine 20 (H4K20Me3) was significantly increased (Fig. 3*D*). Of note, this specific histone modification is often enriched at pericentric heterochromatin, at imprinted genomic regions, and near intracisternal A-particle retrotransposons, commonly demarking constitutive heterochromatin (19).

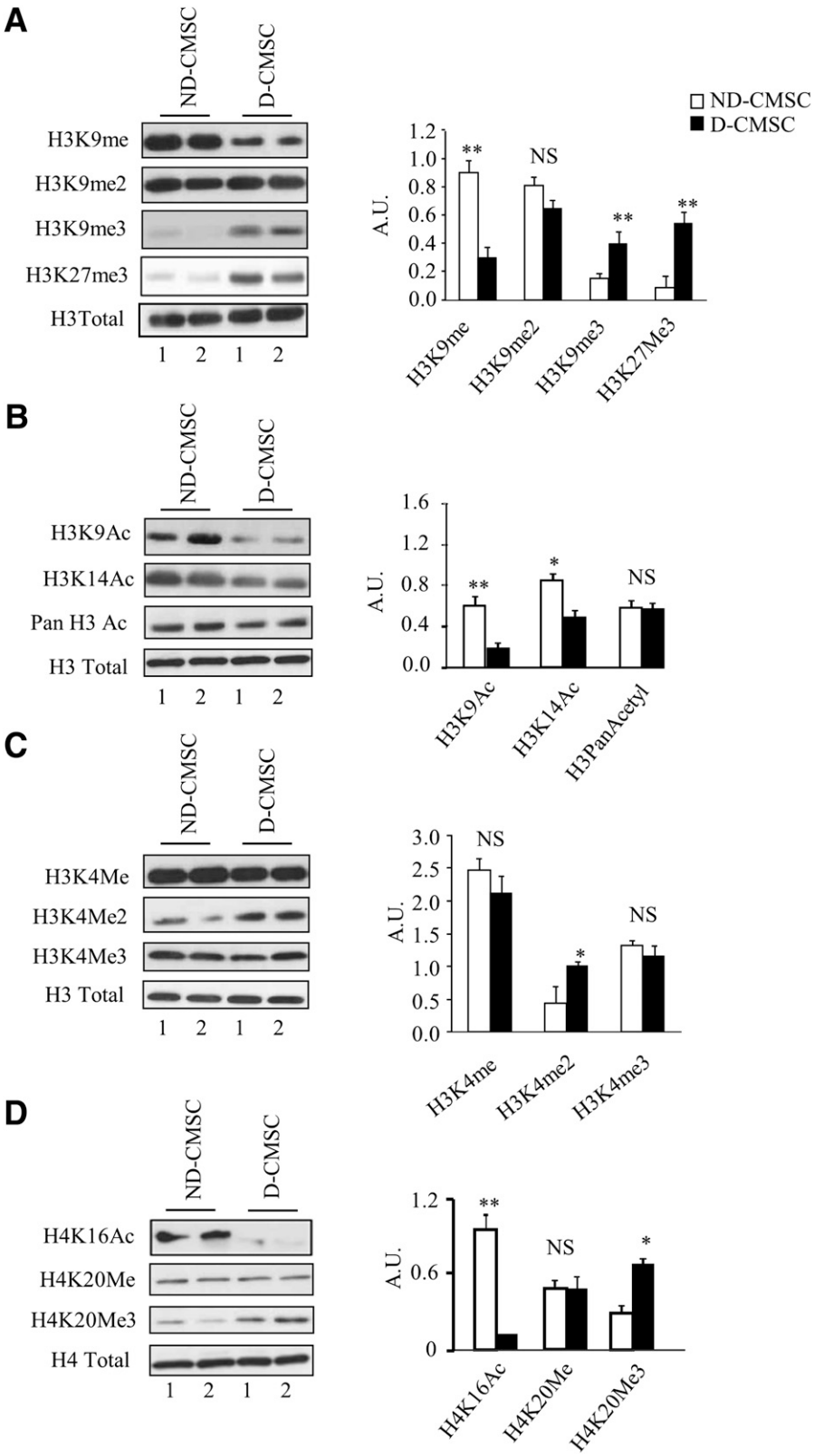


**Figure 3**—Histone code profiling of ND-CMSC and D-CMSC. Representative Western blot analyses show the global histone modification pattern in ND-CMSC compared with D-CMSC. *A*: H3 modifications on lysine (K) 9 and 27: specifically H3K9Me, H3K9Me2, H3K9Me3, H3K27me3. *B*: H3 modifications on K9 and K14: specifically H3K9Ac, H3K14Ac, pan H3Ac. *C*: H3 modifications on K4: specifically H3K4Me, H3K4Me2, and H3K4Me3. *D*: H4 modifications on K16 and 20: specifically H4K16Ac, H4K20Me, and H4K20Me3. The same filter was probed with antitotal histone H3 or H4, respectively, to show equal nuclear protein loading. Band density is depicted on the *right* ($n = 5$ for each group). Each Western blot has been repeated twice in duplicate. $^{**}P \leq 0.01$, $^{*}P \leq 0.05$; A.U., arbitrary units; NS, not significant.

### Epigenetic Enzymes Are Differentially Expressed Between ND-CMSC and D-CMSC

In association with the histone code modifications, the expression of a number of relevant epigenetic enzymes was examined. Figure 4*A* shows that the mRNA levels of Aurora B and C kinases, involved in cell cycle progression, were decreased ~10.8- and 5.7-fold, respectively, in D-CMSC compared with ND-CMSC. This observation may explain the reduced proliferation rate observed in D-CMSC and shown in Fig. 1*A*. Coincidently, in D-CMSC the mRNA level of histone demethylase jmjd3 and the GNAT acetylases GCN5 and p300/CBP-–associated factor (PCAF) were downregulated, about 4.7-, 2.3-, and 2.5-fold. respectively. Class I, II, and III histone deacetylases were

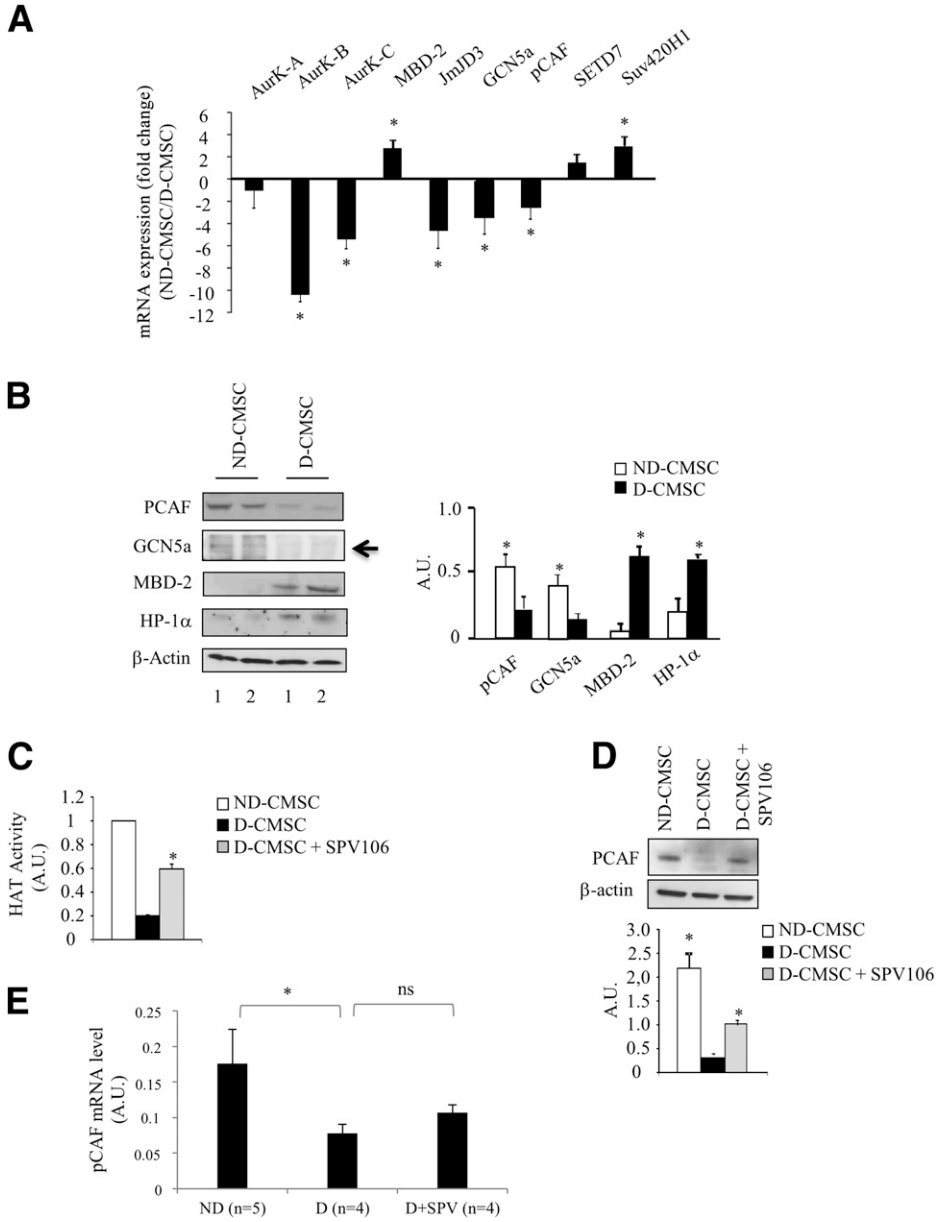


**Figure 4—**Analysis epigenetic enzymes expression. *A*: Real-time RT-PCR analysis was performed to evaluate expression of Aurora (Aur) A, B, and C, PCAF, MBD-2, jmjd3, GCN5, SETD7, and Suv420H1 ($n = 6$). *$P \leq 0.05$. Data are expressed as the ND-CMSC–to–D-CMSC ratio. The graph represents the fold change ± SD of six independent experiments performed in duplicate. *B*: Immunoblot shows expression of PCAF, MBD-2, HP-1α, and GCN5a ($n = 3$). A black arrow indicates the appropriate GCN5a band of 95 kD. The bar graph represents average band density normalized to β-actin. *$P \leq 0.05$. *C*: Total HAT activity measured in ND-CMSC, D-CMSC, and D-CMSC treated with SPV106 ($n = 4$). *$P \leq 0.05$. *D*: Western blot analysis of PCAF protein on ND-CMSC, D-CMSC, and D-CMSC treated with SPV106 for 7 days (*upper*) and relative band density ($n = 3$) (*lower*). *$P \leq 0.05$. *E*: qRT-PCR analysis of PCAF mRNA level in ND-CMSC (ND), D-CMSC (D), and D-CMSC treated with SPV106 (D+SPV) for 7 days ($n = 4$ or 5, as indicated). The results represent the mean ± SEM of each group ($n = 4$ or 5 as indicated). *$P \leq 0.05$; ns, not significant. A.U., arbitrary units.

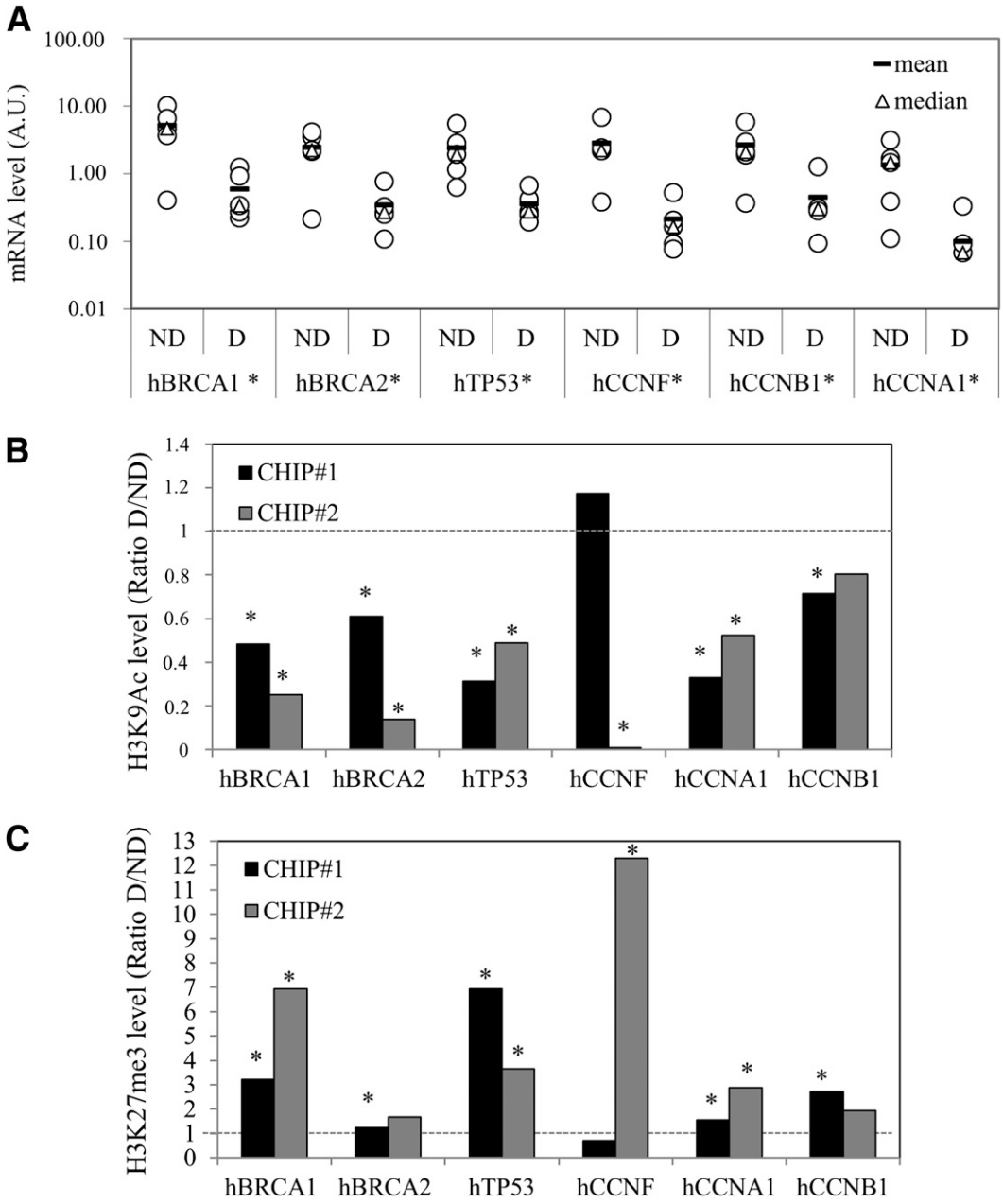


**Figure 5—** Gene expression and ChIP. *A*: mRNA levels were assessed by quantitative PCR in ND-CMSC (ND; $n = 5$) and D-CMSC (D; $n = 5$). Results represent the mean of two independent experiments, each performed in duplicate. The mean and median of each group (ND and D) are indicated. *$P < 0.05$ ND vs. D. *B* and *C*: Two independent ChIP assays (ChIP#1 and #2) were performed using two different ND-CMSC and D-CMSC preparations. Immunoprecipitations were with antibodies to H3K9Ac (*B*) or H3K27me3 (*C*). Recruitment onto promoters was detected by qPCR. Data are expressed as the D-CMSC–to–ND-CMSC ratio (Ratio D/ND) determined after subtraction of no antibody values. The dashed lines depict H3K9Ac (*B*) or H3K27me3 (*C*) levels in ND-CMSC placed equal to 1. *$P < 0.05$ D vs ND. A.U., arbitrary units.

unchanged (data not shown). Accordingly, total histone deacetylases activity was similar in HUVEC with or without high glucose (Supplementary Fig. 3*D*).

On the contrary, histone methylases Suv420H1 (involved in H4K20 methylation), SETD-7, and the methyl CpG binding protein-2 (MBD-2) were upregulated about 3.9-, 2.1-, and 2.4-fold, respectively, in D-CMSC compared with ND-CMSC (Fig. 4*A*). Protein level analysis further confirmed the increase of MBD-2 and that of heterochromatin protein-1 (HP-1), whereas PCAF and GCN5a were reduced in D-CMSC protein extracts (Fig. 4*B*).

The proacetylation compound SPV106 has been described as an activator of the GCN5A/PCAF members of the GNAT family (20) and able to promote histone and nonhistone proteins acetylation (12). In our experiments, D-CMSC were cultured for ~6–8 days in the presence or

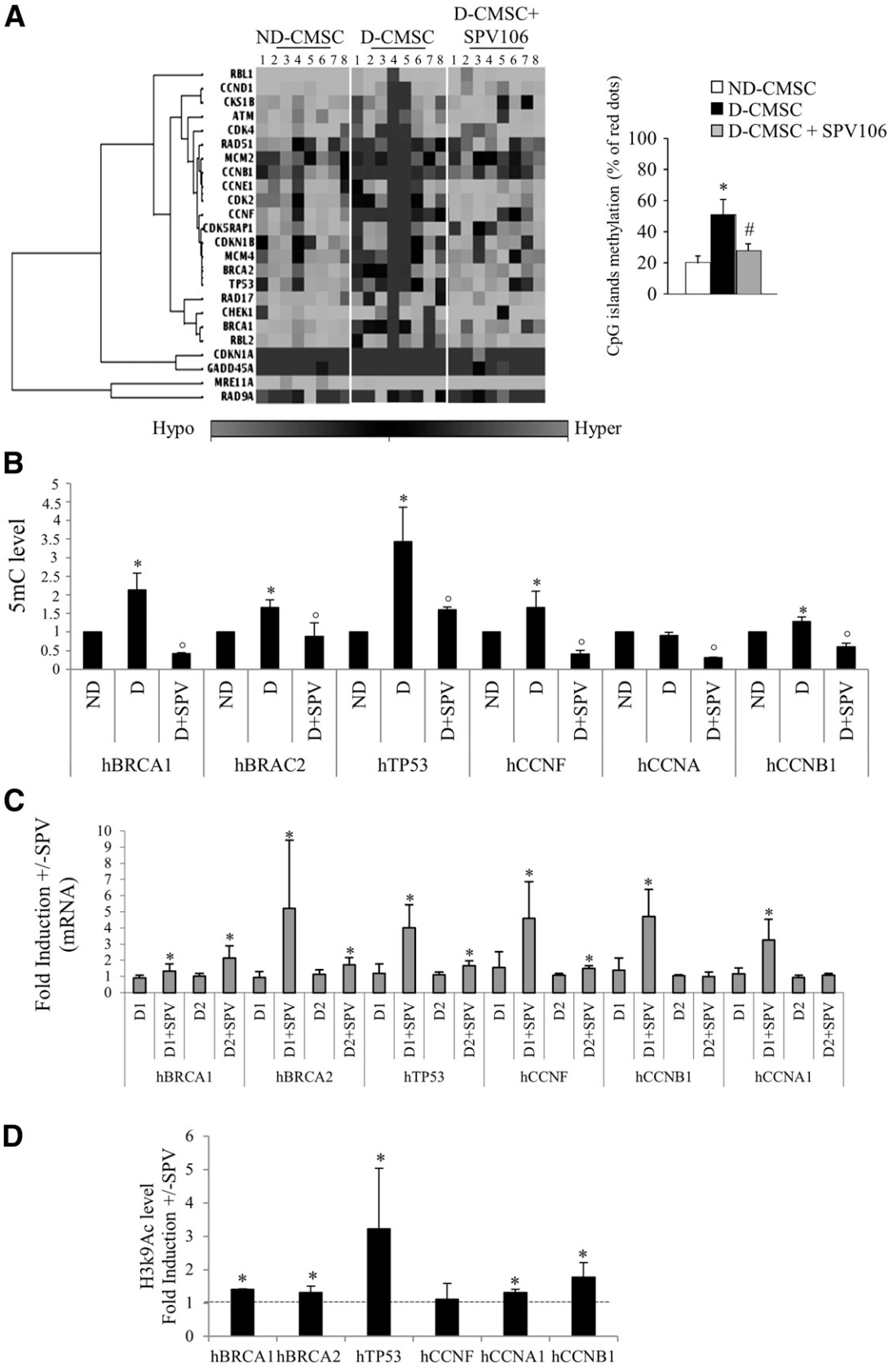


**Figure 6—**Effect of SPV106 treatment on DNA methylation gene expression and histone acetylation at specific promoters. *A*: Methylation profiling of cell cycle and DNA repair gene promoters in ND-CMSC, D-CMSC, and D-CMSC treated with SPV106 (light gray, hypomethylation; black, methylation; dark gray, hypermethylation) (*left*) and quantification of methylation (%) ($n$ = 8) (*right*). *#$P \leq 0.05$. *B*: MeDIp analysis in ND-CMSC, D-CMSC, and D-CMSC treated with SPV. ChIP was performed with antibody to 5-methylcytidine (5mC) or with no

absence of SPV106 at 25 μmol/L, a concentration established in a prior work (21). Partial but significant rescue (62 ± 5%; $P \leq 0.05$) of HAT activity (Fig. 4*C*) was achieved, paralleled by an increase in PCAF protein expression (Fig. 4*D*). This effect was not associated to a rescue in gene transcription as indicated by the quantitative RT-PCR experiment depicted in Fig. 4*E*, thus indicating that posttranscription/translation mechanisms may be involved in this process. Total histone deacetylases expression and activity was unchanged (data not shown and Supplementary Fig. 3*D*).

### Growth Control and DNA Repair Genes Are Hypermethylated in D-CMSC and Rescued by SPV106

The expression of genes known to be associated with proliferation and genome stability was explored at the mRNA level by qRT-PCR. Figure 5*A* shows, in fact, a significant reduction of BRCA1, BRCA2, p53, cyclin F, cyclin B1, and cyclin A transcripts. Figure 5*B* and *C* show representative ChIP experiments performed on two independent groups of CMSC in which the content of H3K9Ac acetylation or lysine 27 trimethylation was explored. The results indicate a consistent reduction of lysine 9 acetylation paralleled by the elevation of lysine 27 trimethylation thus confirming at single gene level, although on a limited number of genomic regions, the observations reported in Fig. 3.

DNA methylation at promoter CpG islands is another important epigenetic modification often associated with histone hypoacetylation, gene repression, and maintenance of a transcription repression state (22). We investigated the CpG islands methylation of gene promoters associated with cell cycle and DNA repair. Remarkably, several of these promoters, including those of TP53, BRCA1 and BRCA2, CCNB1, CCNF, CDK2, MCM2, and RAD5 were found hypermethylated (Fig. 6*A*). These observations suggest that multiple epigenetic modifications take place in D-CMSC involving proliferation and DNA repair genes, although other categories remained unexplored and cannot be excluded. Further investigations are required to elucidate this important point.

DNA hypermethylation of genes associated to proliferation and genomic stability significantly diminished in D-CMSC cultured for 7 days in the presence of SPV106 (Fig. 5*A*). Specifically, after SPV106 treatment, the signal intensity from methylated CpG islands in D-CMSC cell cycle gene promoters shifted from 49.0 ± 13.9% to 21.4 ± 4.8% ($P \leq 0.01$), with an average decrease of about 44%. The effect of SPV106 on DNA methylation was further explored at the single gene level by MeDIp. Figure 6*B* shows that a significant increase in DNA methylation is detectable at the single gene level in cells derived from diabetic patients and that this alteration is reversible after SPV106 treatment. In this condition, the relative gene expression is increased, as shown in Fig. 6*C*, a phenomenon paralleled by a small but significant increment of H3K9Ac (Fig. 6*D*).

This result suggests that histone acetylation and DNA CpG island methylation are in close functional relationship (23). Alterations of the mechanisms involved in their regulation may contribute to establish epigenetic memory in CMSC.

### HAT Activator SPV106 Rescues Proliferation and Differentiation in D-CMSC

In this condition, several histone modifications associated with a chromatin open configuration, in particular H3K9Ac, H3K14Ac (Fig. 7*A*), and H4K16Ac (Fig. 7*B*), reverted to control level. However, the transcription inhibition markers H3K9Me3, H3K27me3, and H4K20me3 were unaffected, suggesting that the global histone methylation level may be insensitive to this proacetylation compound. Remarkably, D-CMSC recovered their proliferation in the presence of SPV106 (Fig. 7*C*), as indicated by cell counting and the increase in H3S10 phosphorylation (Fig. 7*A*). Similar evidence was obtained in HUVEC exposed to high glucose where SPV106 treatment induced the acetylation of H3K9 (Supplementary Fig. 4*A* and *B*), rescuing HAT activity and cell proliferation (Supplementary Fig. 4*C* and *D*).

In the same condition, SPV106 did not significantly change cellular respiration and glycolysis in ND-CMSC or D-CMSC, although it demonstrated a positive trend in this direction (Supplementary Fig. 5*A*–*H*). However, the cellular content of ATP was significantly increased in D-CMSC compared with ND-CMSC. Treatment of 7 days with SPV106 normalized ATP levels (Supplementary Fig. 5*I*).

Of note, D-CMSC did not recover adipogenic differentiation (data not shown) in the presence of SPV106, whereas the capillary-like structure formation evaluated by Cultrex assay (Fig. 7*D*) was significantly restored as in HUVEC (Supplementary Fig. 4*E*).

### SPV106 Reduces Cellular Senescence and Induces cKit Expression in D-CMSC

The SPV106 compound is known to be active on the PCAF/GCN5a HAT family. To further explore its effects

specific primary antibody added in each condition tested. Sonicated and immunoprecipitated fragments were amplified by qPCR using specific primers (see RESEARCH DESIGN AND METHODS). Data, expressed as fold change vs. ND, represent the mean ± SD of two independent experiments performed in duplicate. *$P < 0.05$ D vs. N; °$P < 0.05$ D+SPV vs. D. *C*: The level of selected mRNAs was assessed by qPCR in two different D-CMSC preparations (D1 and D2) before and after treatment with SPV106 (SPV). Results are plotted as fold induction (±SPV) and represent the mean ± SD of two independent experiments performed in duplicate. *$P < 0.05$ D+SPV vs. D. *D*: ChIP assay was performed by using a specific antibody to histone H3K9Ac or in absence of primary antibody (no antibody). The experiment was performed with two different D-CMSC preparations. Recruitment onto promoters was detected by qPCR. Data are expressed as the D-CMSC+SPV–to–D-CMSC ratio determined after subtraction of the no antibody values. The dashed line represents H3K9Ac levels in untreated D-CMSC placed equal to 1. *$P < 0.05$.

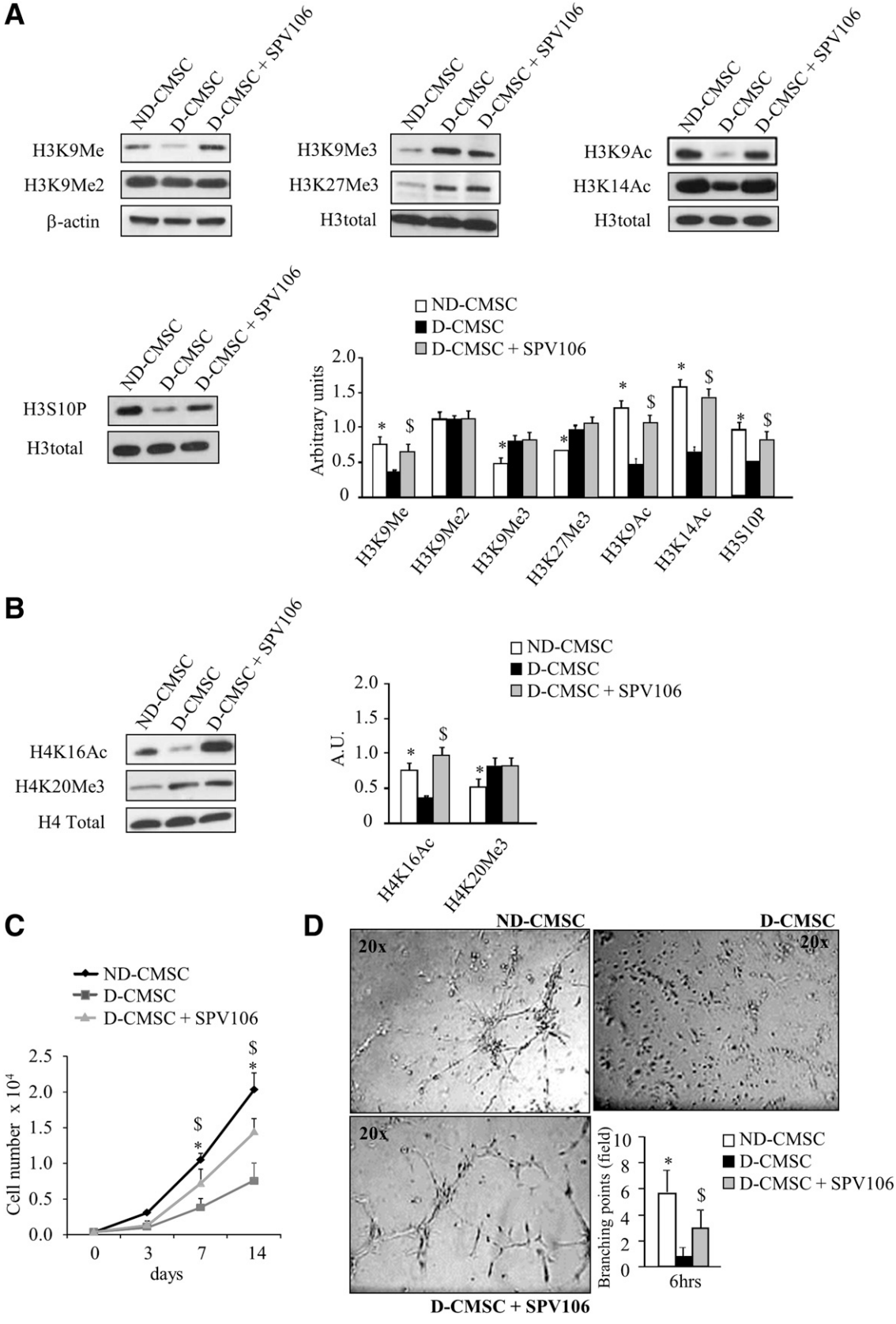


**Figure 7**—SPV106 treatment restores normal-like epigenetic profile and cellular function in D-CMSC. *A*: Western blot analysis on histone proteins after SPV106 treatment on D-CMSC compared with D-CMSC and ND-CMSC. The following H3 modifications were evaluated: H3K9Me and H3K9Me2 (*upper left*), H3K9Me3 and H3K27me3 (*upper middle*), H3K9Ac and H3K14Ac (*upper right*), and H3S10P (*lower left*). Antitotal histone H3 or β-actin was used to show equal protein loading. The bar graph (*lower right)* depicts the relative band density

on CMSC, experiments were performed to evaluate acidic β-galactosidase content in D-CMSC at passage 8 and cultured for 7 days in the presence of the drug. Figure 8*A* shows that acidic β-galactosidase accumulation was reduced approximately twofold in the presence of SPV106.

Garcinol is a natural product known as a potent HAT inhibitor active on PCAF/GCN5a and p300 (24). It has been recently described to largely reproduce in vivo the cardiovascular phenotype detectable in PCAF knockout mice (24). We used garcinol on ND-CMSC to evaluate the effect of a reduced HAT activity on these cells. Figure 8*B* (*left*) shows that ND-CMSC do not efficiently proliferate in the presence of garcinol, with a shape similar to that of untreated D-CMSC (see Fig. 1*A* and Fig. 7*C*). Moreover, Fig. 8*B* (*right*) shows that ND-CMSC exposed to garcinol revealed a significantly higher content of acidic β-galactosidase at the 7-day time point, thus reproducing the senescent phenotype observed in D-CMSC (Fig. 1*B* and Fig. 8*A*).

The PCAF/GCN5a family contributes to histone and nonhistone protein acetylation. To evaluate this aspect, a Western blotting analysis was performed on ND-CMSC treated with SPV106 or garcinol, its functional counterpart. Figure 8*C* (*left*) indicates that SPV106 slightly increases tubulin acetylation, a process counteracted by garcinol. As previously reported (11), ND-CMSC are sensitive to EpiC, whereas D-CMSC are less prone to differentiate in this condition (see also Fig. 2*B*). In this work, the effect of garcinol and SPV106 was tested on ND-CMSC and D-CMSC, respectively, in addition to EpiC treatment, and found that cKit expression was enhanced by SPV106 treatment in D-CMSC cells but was abolished by garcinol in ND-CMSC. This result supports the relevance of an optimal level of HAT activity in CMSC during the differentiation process.

## DISCUSSION

In the present work, we characterized CMSC obtained from patients with and without diabetes undergoing CABG. CMSC from diabetic patients revealed a reduction in proliferation (3.5-fold less then control patients, on average), possibly reflecting the ongoing acquisition of a premature senescent phenotype associated with a compromised differentiation potential. In light of this evidence, we hypothesized that these cells acquired important epigenetic changes (22). To explore this possibility, the epigenetic landscape of CMSC was investigated, focusing on cells that could have been exposed to altered metabolic conditions for several years (see Supplementary Table 1). In our patient population, in fact, diabetes was diagnosed from 3 to 17 years before the worsening of their cardiac symptoms required cardiac surgery. Epigenetic differences were observed compared with cells derived from normoglycemic control subjects. Specifically, D-CMSC revealed the predominance of transcription repressive markers, including the increase of H3K9Me3, H3K27me3, and H3K20Me3, and a significant decrease of histone modifications (H3K9Ac and H4K16Ac) often associated with an accessible chromatin structure. The evaluation of epigenetic enzymes expression, such as that of GCN5a, PCAF, jmjd3, and HP-1a, highlighted a specific signature associated with D-CMSC, well reproducible in cells isolated from different patients. Remarkably, histone modifications and epigenetic enzymes expression were paralleled by DNA methylation, a modification contributing to gene repression (25,26). In light of these findings, we investigated the level of CpG island methylation at cell cycle gene promoters and found a profile consistent with the reduced proliferation rate observed in D-CMSC (27).

Prior observations indicated that the HAT activator SPV106 was proficient at promoting histone acetylation in normal and physiopathological conditions (23,28,29). In this study, we wished to investigate whether D-CMSC could be sensitive to the increase of histone acetylation levels. In the presence of SPV106, proliferation and differentiation were rescued in most D-CMSC cells. A large number of epigenetic modifications, including histones and DNA methylation, were also significantly normalized. Similar results were obtained in HUVEC exposed to high glucose, as shown in Supplementary Figs. 2, 3 and 4, indicating that the metabolic environment created by the increase in glucose levels could be involved in the establishment of persistent functional cellular defects in CMSC. Although the limited number of samples analyzed indicated a not significant alteration in cellular respiration and glycolysis in D-CMSC versus ND-CMSC, a positive trend could be assigned to the effect of SPV106 on these two metabolic parameters. Of major interest is the observation that the total ATP content is increased in D-CMSC and that this alteration is prevented by SPV106 treatment. An increased ATP content has been recently associated with the onset of insulin resistance in obese patients as a possible marker of T2D predisposition (11,30). Further research will be necessary to investigate the potential metabolic effect of lysine acetylation in the onset of insulin resistance and diabetes.

($n = 3$). *$P \leq 0.05$, $NS vs. ND-CMSC. A.U., arbitrary units. *B*: Western blot analysis on histone H4 after SPV106 treatment on D-CMSC compared with D-CMSC and ND-CMSC. H4K16Ac and H4K20Me3 were evaluated. Antitotal H4 has been used to show equal protein loading ($n = 3$). *$P \leq 0.05$, $NS vs. ND-CMSC. *C*: Growth curve analysis on ND-CMSC, D-CMSC, and D-CMSC treated with SPV106. Cells were cultured for 14 days. Graph shows the mean ± SD of five independent experiments ($n = 7$, for each group). *$P \leq 0.05$, $NS vs. ND-CMSC. *D*: Representative photomicrographs of Cultrex assay performed with ND-CMSC, D-CMSC, and D-CMSC cultured in the presence of endothelial cell growth media-2 for 14 days. D-CMSC were treated with SPV106 or equivalent amount of solvent for 1 additional week. The bar graph shows formation of capillary-like structures measured as the count of branching points per field ($n = 4$). *$P \leq 0.05$, $NS vs. ND-CMSC.

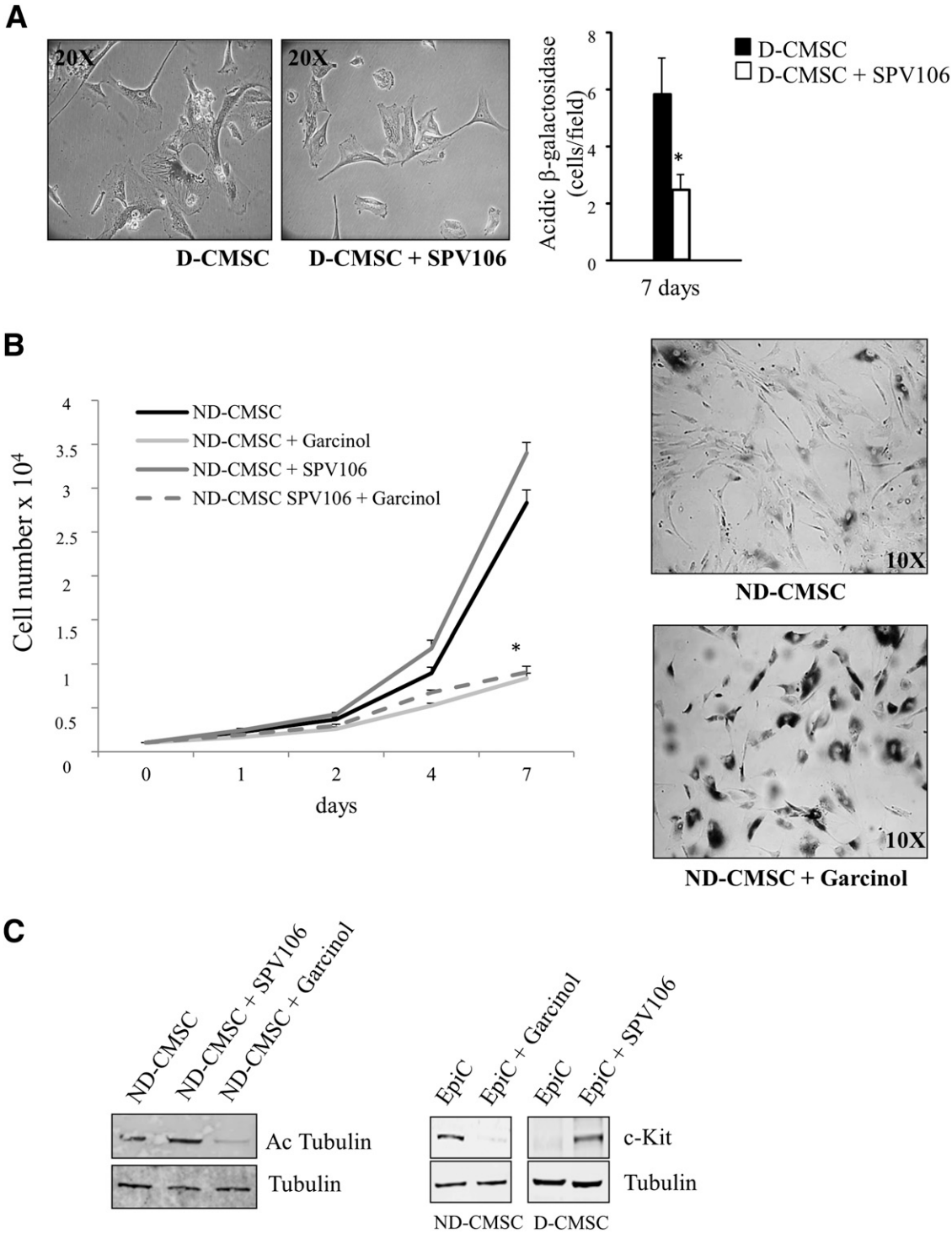


**Figure 8**—SPV106 and garcinol provide opposing signals in CMSC. *A*: Representative photomicrographs of D-CMSC culture in the presence or absence of SPV106. D-CMSC were kept in growth medium and passaged up to passage 8. SPV106 (5 μmol/L) or equivalent amount of solvent were added every 2 days. The presence of cellular senescence (black cells) was detected by the acidic β-galactosidase assay. The bar graph shows the average number of senescent cells per field in the presence or absence of SPV106. Counts were performed in 10 different fields. The experiment was repeated twice with three distinct D-CMSC preparations. *$P \leq 0.05$. *B*: Graph depicts the average effect of SPV106, garcinol, or both in combination on passage 3 ND-CMSC cultured for 7 days in growth medium. The experiment was repeated twice in duplicate on two different cell preparations. *$P \leq 0.005$. Representative photomicrographs (*right*) of passage 3 ND-CMSC cultured for 7 days in the presence or absence of garcinol (5 μmol/L). The black staining (*lower right*) identifies senescent β-galactosidase–positive cells. *C*: Western blotting analysis of acetylated α-tubulin (*left*) in ND-CMSC treated 24 h with SPV106 or garcinol. Equivalent amounts of solvent were added to controls (ND-CMSC). Data indicate that SPV106 induces α-tubulin acetylation, which is reduced by garcinol. The *right* panels show the effect of garcinol in cells treated with EpiC (14). In the presence of garcinol, the expression of the differentiation marker cKit is abrogated in ND-CMSC, whereas SPV106 rescues cKit expression in D-CMSC.

A remarkable result of this study, however, is that the lysine hyperacetylation induced by SPV106 determined a significant modification in DNA methylation level. A growing body of literature indicates that lysine acetylation and DNA methylation are in functional relationship and that increasing acetylation may determine a reduction in methylated DNA content (31,32). The recent work of Qian et al. (23) demonstrates that a histone acetyltransferase regulates the level of DNA methylation in *Arabidopsis thaliana*, inducing acetylation-dependent DNA demethylation. Whether this mechanism is involved in the regulation of cell cycle and DNA repair genes in D-CMSC is still unclear. However, the acetylation-dependent demethylation determined by SPV106 treatment suggests that HATs are involved in this process. Further experiments are required to elucidate this important point.

In conclusion, diabetes alters the metabolic milieu determining long-term changes in the epigenetic landscape with important consequences on cellular function. Targeted epigenetic interventions may contribute to recover the altered chromatin state, indicating new epigenetically based potential therapeutic strategies aimed at ameliorating stem cell performances in diabetic patients and, consequently, counteracting diabetes complications.

**Funding.** The current study was supported by the Italian Ministry of Health and by the Italian Ministry of Education, Universities and Research (FIRB-MIUR RBFR10URHP to S.N., FIRB-MIUR RBFR087JMZ to A.R. and A.F., and PRIN2010-TYCL9B_006 to A.F.). C.G. is supported by the LOEWE-CGT Centre of Excellence, Wolfgang Goethe University. F.S. is supported by LOEWE-CGT Center, Wolfgang Goethe University, and by LOEWE-CGT grant III L4 517/17004.

The funders had no role in study design, data collection and analysis, decision to publish, or preparation of the manuscript.

**Duality of Interest.** A.D. was funded by Fresenius Medical Care Deutschland GmbH. No other potential conflicts of interest relevant to this article were reported.

**Author Contributions.** M.V., F.S., S.N., C.Co., G.S., A.M., G.P., M.C.Cap., A.R., S.D., A.Z., and C.G. conceived and designed the experiments. M.V., F.S., S.N., C.Co., C.Ce., A.D., M.T., and M.C.Car. performed the experiments. M.V., F.S., S.N., C.Co., C.Ce., A.D., M.T., M.C.Car., G.S., S.C., A.M., F.M., A.R., S.D., A.Z., and C.G. analyzed the data. S.N., C.Co., B.B., A.F., G.S., S.C., A.M., G.P., A.Z., and C.G. contributed the reagents, materials, and analysis tools. M.V., F.S., S.N., A.F., and C.G. wrote the manuscript. C.G. is the guarantor of this work and, as such, had full access to all the data in the study and takes responsibility for the integrity of the data and the accuracy of the data analysis.

## References

1. Ershow AG. Environmental influences on development of type 2 diabetes and obesity: challenges in personalizing prevention and management. J Diabetes Sci Tech 2009;3:727–734

2. Mangiapane H. Cardiovascular disease and diabetes. Adv Exp Med Biol 2012;771:219–228

3. Jouven X, Lemaître RN, Rea TD, Sotoodehnia N, Empana JP, Siscovick DS. Diabetes, glucose level, and risk of sudden cardiac death. Eur Heart J 2005;26:2142–2147

4. Herlitz J, Malmberg K. How to improve the cardiac prognosis for diabetes. Diabetes Care 1999;22(Suppl. 2):B89–B96

5. El-Helou V, Proulx C, Béguin P, et al. The cardiac neural stem cell phenotype is compromised in streptozotocin-induced diabetic cardiomyopathy. J Cell Physiol 2009;220:440–449

6. Fadini GP, Miorin M, Facco M, et al. Circulating endothelial progenitor cells are reduced in peripheral vascular complications of type 2 diabetes mellitus. J Am Coll Cardiol 2005;45:1449–1457

7. Gallagher KA, Liu ZJ, Xiao M, et al. Diabetic impairments in NO-mediated endothelial progenitor cell mobilization and homing are reversed by hyperoxia and SDF-1 alpha. J Clin Invest 2007;117:1249–1259

8. Creager MA, Lüscher TF, Cosentino F, Beckman JA. Diabetes and vascular disease: pathophysiology, clinical consequences, and medical therapy: Part I. Circulation 2003;108:1527–1532

9. Rossini A, Frati C, Lagrasta C, et al. Human cardiac and bone marrow stromal cells exhibit distinctive properties related to their origin. Cardiovasc Res 2011;89:650–660

10. Dominici M, Le Blanc K, Mueller I, et al. Minimal criteria for defining multipotent mesenchymal stromal cells. The International Society for Cellular Therapy position statement. Cytotherapy 2006;8:315–317

11. Vecellio M, Meraviglia V, Nanni S, et al. In vitro epigenetic reprogramming of human cardiac mesenchymal stromal cells into functionally competent cardiovascular precursors. PLoS ONE 2012;7:e51694

12. Milite C, Castellano S, Benedetti R, et al. Modulation of the activity of histone acetyltransferases by long chain alkylidenemalonates (LoCAMs). Bioorg Med Chem 2011;19:3690–3701

13. Spallotta F, Cencioni C, Straino S, et al. Enhancement of lysine acetylation accelerates wound repair. Commun Integr Biol 2013;6:e25466

14. Nanni S, Benvenuti V, Grasselli A, et al. Endothelial NOS, estrogen receptor beta, and HIFs cooperate in the activation of a prognostic transcriptional pattern in aggressive human prostate cancer. J Clin Invest 2009;119:1093–1108

15. Re A, Aiello A, Nanni S, et al. Silencing of GSTP1, a prostate cancer prognostic gene, by the estrogen receptor-β and endothelial nitric oxide synthase complex. Mol Endocrinol 2011;25:2003–2016

16. Lee OK, Kuo TK, Chen WM, Lee KD, Hsieh SL, Chen TH. Isolation of multipotent mesenchymal stem cells from umbilical cord blood. Blood 2004;103:1669–1675

17. He JQ, Vu DM, Hunt G, Chugh A, Bhatnagar A, Bolli R. Human cardiac stem cells isolated from atrial appendages stably express c-kit. PLoS ONE 2011;6:e27719

18. Claycomb WC, Lanson NA Jr, Stallworth BS, et al. HL-1 cells: a cardiac muscle cell line that contracts and retains phenotypic characteristics of the adult cardiomyocyte. Proc Natl Acad Sci U S A 1998;95:2979–2984

19. Wongtawan T, Taylor JE, Lawson KA, Wilmut I, Pennings S. Histone H4K20me3 and HP1α are late heterochromatin markers in development, but present in undifferentiated embryonic stem cells. J Cell Sci 2011;124:1878–1890

20. Vetting MW, S de Carvalho LP, Yu M, et al. Structure and functions of the GNAT superfamily of acetyltransferases. Arch Biochem Biophys 2005;433:212–226

21. Colussi C, Rosati J, Straino S, et al. Nε-lysine acetylation determines dissociation from GAP junctions and lateralization of connexin 43 in normal and dystrophic heart. Proc Natl Acad Sci U S A 2011;108:2795–2800

22. El-Osta A, Brasacchio D, Yao D, et al. Transient high glucose causes persistent epigenetic changes and altered gene expression during subsequent normoglycemia. J Exp Med 2008;205:2409–2417

23. Qian W, Miki D, Zhang H, et al. A histone acetyltransferase regulates active DNA demethylation in Arabidopsis. Science 2012;336:1445–1448

24. Bastiaansen AJ, Ewing MM, de Boer HC, et al. Lysine acetyltransferase PCAF is a key regulator of arteriogenesis. Arterioscler Thromb Vasc Biol 2013;33:1902–1910

25. Hackett JA, Surani MA. DNA methylation dynamics during the mammalian life cycle. Philos Trans R Soc Lond B Biol Sci 2013;368:20110328

26. Ng SF, Lin RC, Laybutt DR, Barres R, Owens JA, Morris MJ. Chronic high-fat diet in fathers programs β-cell dysfunction in female rat offspring. Nature 2010;467:963–966

27. Berdasco M, Esteller M. DNA methylation in stem cell renewal and multipotency. Stem Cell Res Ther 2011;2:42
28. Colussi C, Scopece A, Vitale S, et al. P300/CBP associated factor regulates nitroglycerin-dependent arterial relaxation by N(ε)-lysine acetylation of contractile proteins. Arterioscler Thromb Vasc Biol 2012;32:2435–2443
29. Wei W, Coelho CM, Li X, et al. p300/CBP-associated factor selectively regulates the extinction of conditioned fear. J Neurosci 2012;32:11930–11941
30. Ye J. Mechanisms of insulin resistance in obesity. Front Med 2013;7:14-24
31. Cervoni N, Detich N, Seo SB, Chakravarti D, Szyf M. The oncoprotein Set/TAF-1beta, an inhibitor of histone acetyltransferase, inhibits active demethylation of DNA, integrating DNA methylation and transcriptional silencing. J Biol Chem 2002;277:25026–25031
32. Cervoni N, Szyf M. Demethylase activity is directed by histone acetylation. J Biol Chem 2001;276:40778–40787